minerals

MDPI

Article

Paleoproterozoic Adakitic Rocks in Qingchengzi District, Northeastern Jiao-Liao-Ji Belt: Implications for Petrogenesis and Tectonism

Jian Li [1,2], Hanlun Liu [3], Keyong Wang [1,*] and Wenyan Cai [1,2]

1 College of Earth Sciences, Jilin University, Changchun 130061, China; lijian17@jlu.edu.cn (J.L.); caiwy17@163.com (W.C.)
2 Resources and Environmental Engineering, Shandong University of Technology, Zibo 255049, China
3 Institute of Mineral Resources, Chinese Academy of Geological Sciences, Beijing 100037, China; p02419@163.com
* Correspondence: wangky@jlu.edu.cn

Received: 21 June 2020; Accepted: 29 July 2020; Published: 31 July 2020

Abstract: Herein, zircon U-Pb geochronology, Lu-Hf isotopes, and whole-rock major and trace element geochemistry are presented for two Palaeoproterozoic granitic rocks in Qingchengzi district, northeastern Jiao-Liao-Ji Belt (JLJB). These new geochronological and geochemical data provide reference clues for exploring the petrogenesis and tectonic setting of Paleoproterozoic magmatic rocks in the Qingchengzi district, which further constrain the tectonic nature of the JLJB. Our zircon U-Pb dating denotes that the Paleoproterozoic magmatic events in the Qingchengzi district were emplaced at ~2163 Ma and ~1854 Ma, represented by granite porphyry and biotite granite, respectively. Geochemically, these Palaeoproterozoic rocks are characterized by high Sr (760–842 ppm), SiO_2 (69.72–70.89 wt.%), and Al_2O_3 (15.53–16.78 wt.%) contents, low Y (2.1–9.0 ppm) and Yb (0.25–0.80 ppm) contents, which indicate an adakite affinity. Combined with Hf isotopic composition ($\varepsilon Hf(t)$ = −1.5~+4.8; T_{DM2} = 3109~2560 Ma), we believe that the Paleoproterozoic adakitic magma originated from partial melting of the thickened lower crust material in the Meso-Neoarchean. Moreover, these rocks are enriched in light rare earth elements and large ion lithophilic elements (e.g., K, Rb, and Cs), and depleted in heavy rare earth elements and high field strength elements (e.g., Nb and Ta). These features are similar to magmatic rocks formed in an arc environment (either island arc or active continental margin) and are not consistent with an intraplate/intracontinental environment. According to this study and previous research results, we conclude that the arc–continent collision model is conducive to the Paleoproterozoic tectonic attribute of the JLJB, and the oceanic crust subduction between the Namgrim and Longgang blocks may have induced the widespread occurrence of magmatic events in the region.

Keywords: geochronology; geochemistry; Qingchengzi district; Jiao-Liao-Ji Belt

1. Introduction

The North China Craton (NCC), located in eastern China, has a long-term and complex geological tectonic evolution. It experienced multistage Archean crustal accretion and reconstruction [1,2]. During the Paleoproterozoic, Ordos, Yinshan, Longgang, and Namgrim microcontinent blocks were aggregated along the orogenic belts, including the Khondalite Belt, Trans-North China Orogen, and Jiao-Liao-Ji Belt, which also marked the completion of cratonization [3–5]. The Paleoproterozoic Jiao-Liao-Ji Belt (JLJB; also called the Liaoji Belt) is located in the Eastern Block of the NCC, elongate domain that trends NE–SW for 700 km from eastern Shandong, through eastern Liaoning and

southern Jilin, in China, and extends into northern North Korea (Figure 1) [3–6]. It is an important Paleoproterozoic orogenic belt connecting the Longgang and Namgrim blocks [3–5,7–10].

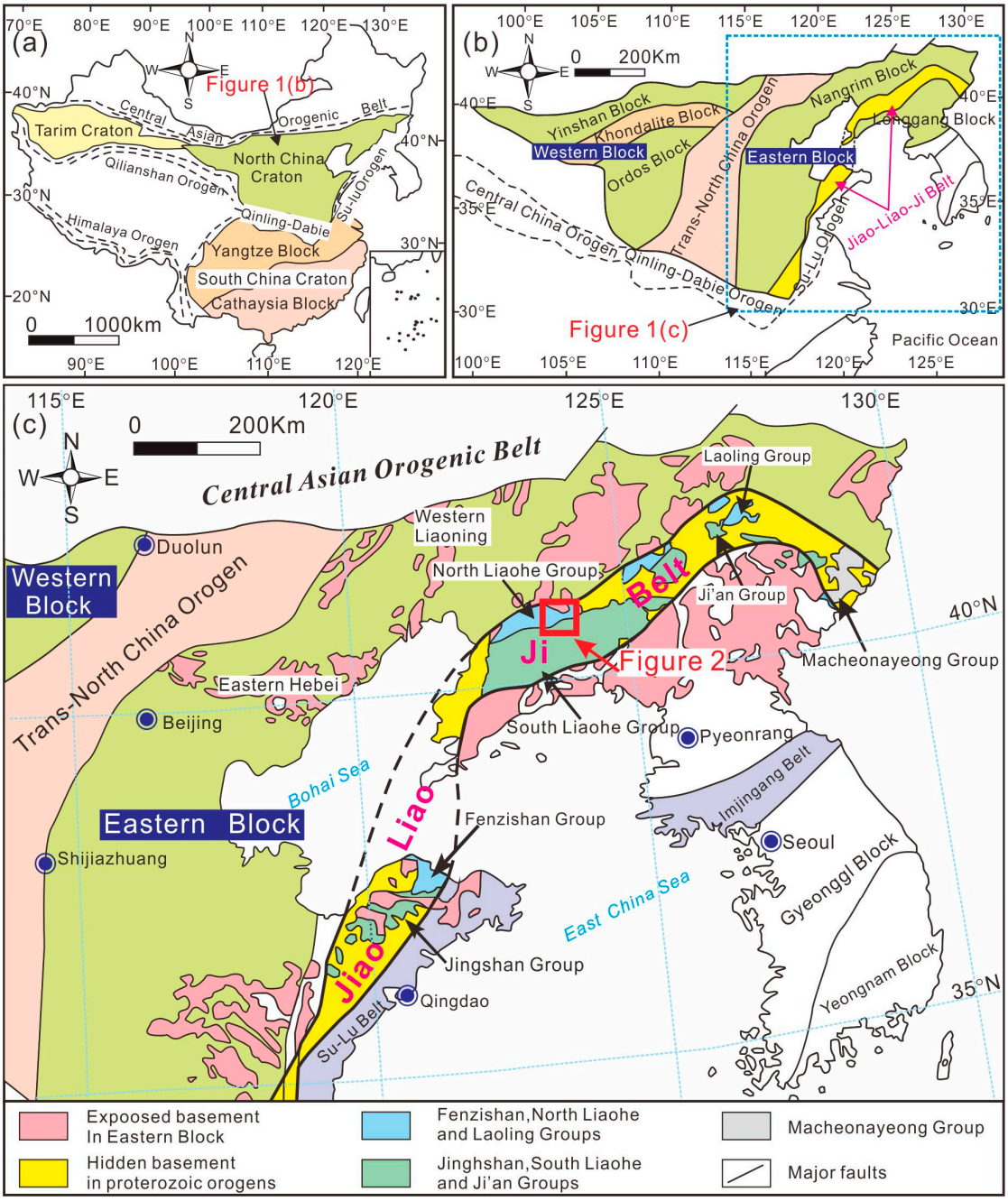

Figure 1. (**a**) Major structural distribution map of China. (**b**) Geological map of the North China Craton, and (**c**) the Paleoproterozoic Jiao-Liao-Ji Belt (after Zhao et al. [3]).

Unlike the other two well-studied Paleoproterozoic orogenic belts [3–5,11–21], whether tectonic properties of the JLJB belong to the intracontinental rift model [22–27] or the arc–continent collision model [28–35], is still a controversial issue. Granitoids provide significant information for lithospheric processes and tectonic settings, particularly about their geochronology and whole-rock geochemistry [36–38]. Paleoproterozoic granitoids are widely exposed in the northeast part of the JLJB, which are called "Liaoji granites" [22,23]. Accurate geochronological and geochemical studies of

these granitoids are of great significance for understanding the tectonic properties of the JLJB and the magmatic events of these Paleoproterozoic granitoids.

In this contribution, we present petrological observations, laser ablation inductively coupled plasma mass spectrometry (LA–ICP–MS) zircon U-Pb dating, Lu-Hf isotope analysis, and whole-rock geochemical studies for the representative Paleoproterozoic granitoids in the Qingchengzi district, northeastern JLJB. These new datasets provide precise age, petrogenesis process, and magma source for the Paleoproterozoic "Liaoji granites," and yield new insights to further constrain the tectonic settings of the JLJB.

2. Geological Setting

2.1. Tectonic Framework

The NCC is the oldest and largest (~1.5 million km^2) cratonic block in East Asia (Figure 1a,b), and the preserved metavolcanic/sedimentary rocks (e.g., orthogneisses and metavolcanic) could date back to the Eoarchean (ca. 3.8 Ga) [18,21,39–42]. The craton extends from western Inner Mongolia in the west to the northern Korean peninsula in the east (Figure 1) [3]. The NCC consists of two parts, the Eastern Block and Western Block, which belong to the Archean–Paleoproterozoic basement and collided with the Trans-North China Orogen (TNCO) at ~1.85 Ga (Figure 1b,c) [3]. The Western Block consists of the Ordos and Yinshan blocks, which collided along the Khondalite Belt (KB) at ~1.95 Ga. The Eastern Block also includes two blocks (Longgang and Namgrim), which are separated by the JLJB (~1.95 Ga; Figure 1b,c) [3,4]. The collage–aggregation of several microcontinent blocks was accompanied by the formation of important tectonic/orogenic belts (i.e., KB, JLJB, and TNCO) that marked the completion of cratonization, and then the craton was in a long-term stable stage until the occurrence of few magmatic events in Mesozoic [43].

2.2. Local Geology and Sample Descriptions

The Qingchengzi district is situated in the northeastern part of the JLJB (Figure 1c). The geological units exposed in this district are mainly the Paleoproterozoic Liaohe Group (metasedimentary rocks) and Quaternary sediments (Figure 2). Within the district, the Liaohe Group can be divided into five formations, including the Gaixian, Dashiqiao, Gaojiayu, Li'eryu (missing in this district), and Langzishan (concealed) from top to bottom (Figure 2). Detailed lithologic and structural features can be seen in Li et al. [44,45]. There are many magmatic events from Paleoproterozoic to Mesozoic in this district, which intruded into Precambrian strata (Figure 2) [43–45]. In this study, the Paleoproterozoic magmatic rocks were collected from the central part of a dike and adjacent isolated large-scale batholith (southeastern) (Figure 2). The detailed petrography is described as follows.

The granite porphyry dikes (labeled as TH samples herein; location: 40°43′45″ N, 123°37′54″ E) are located in the central part of the district. The granite porphyry is characterized by a porphyritic texture and massive structure. Petrographic observations show that the phenocrysts (~45%) are mainly plagioclase (25%), alkali feldspar (10%), quartz (5%), and biotite (3–5%). The matrix (~55%) mineral assemblages are mainly alkali feldspar, plagioclase, and quartz. Minor accessory minerals (~1%) such as zircon and sphene are also developed in this rock. In general, the quartz in the phenocrysts developed weak dissolution pores, and the plagioclase has weak sericitization (Figure 3a,b).

The biotite granite (labeled as DDZ samples herein; location: 40°42′40″ N, 123°40′19″ E) is located in the southeast part of the district. Petrographically, the biotite granite has a fine-grained texture and massive structure. The mineral assemblages of biotite granite are mainly plagioclase (35–40%), quartz (~30%), alkali feldspar (20–25%), biotite (>5%), and accessory minerals (~1%; mainly zircon) (Figure 3c,d).

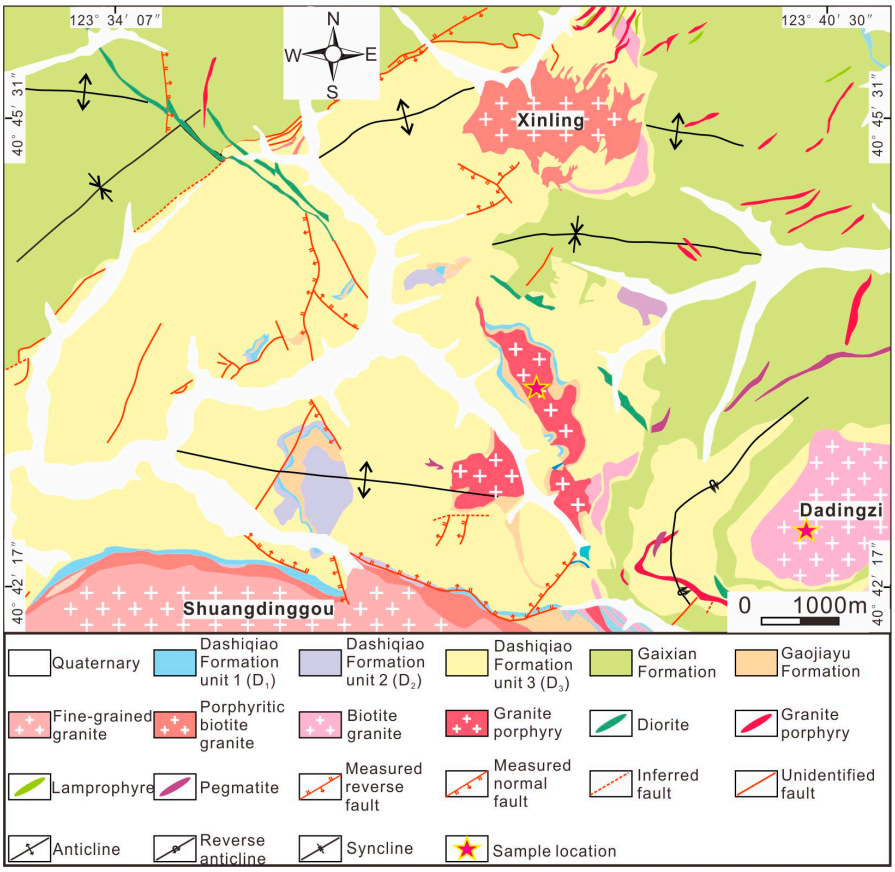

Figure 2. Geological map of the Qingchengzi district (after Li et al. [44]).

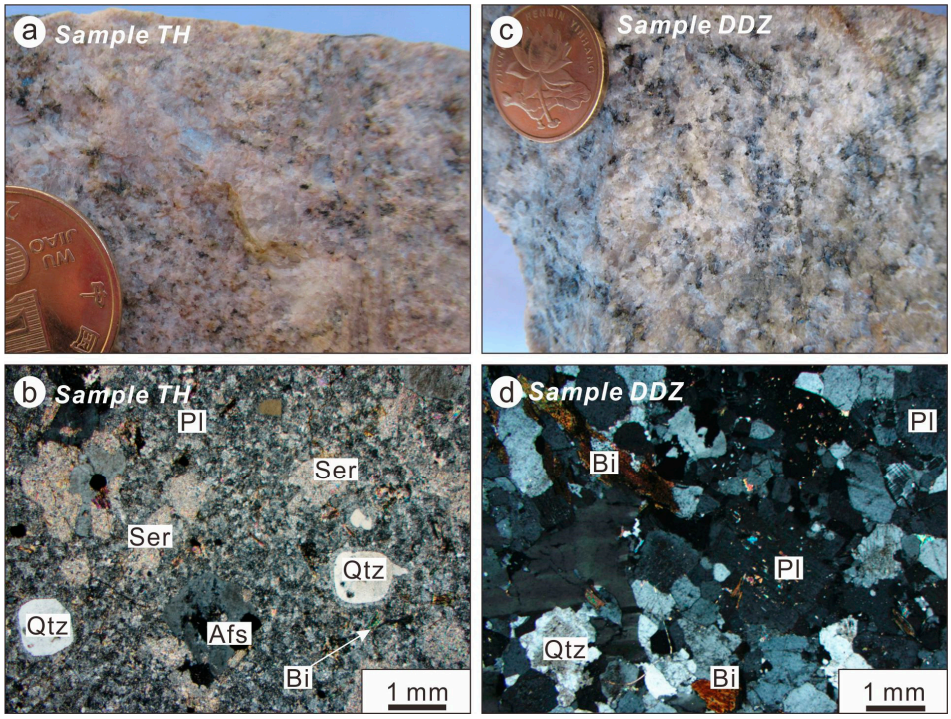

Figure 3. Hand specimens and microphotographs (cross-polarized light) of the Paleoproterozoic magmatic rocks in Qingchengzi district. (**a**,**b**) granite porphyry; (**c**,**d**) biotite granite. Abbreviations: Qtz = quartz; Afs = alkali feldspar; Ser = sericitization; Pl = plagioclase; Bi = biotite.

3. Analytical Techniques

3.1. Zircon U-Pb Dating

We collected two samples of granite porphyry (sample TH) and biotite granite (sample DDZ) for LA–ICP–MS zircon U-Pb geochronology analysis. In Langfang Sincerity Geological Service Co. Ltd, the conventional heavy liquid and magnetic technologies were used to complete the separation of zircon grains. The cathodoluminescence (CL) images were performed by Quanta 200F ESEM (scanning electron microscope) at Sample Solution Analytical Technology Co. Ltd (Wuhan, China). Transparent and uncracked zircons, or those free of inclusions, were selected for age determination.

Using an Agilent 7500c quadrupole ICP–MS, automatic positioning system, and 193 nm ArF excimer laser (COMPexPro 102, Coherent, DE), zircon U-Pb geochronology data were collected in the Key Laboratory of Mineral Resources Evaluation in Northeast Asia, Ministry of Land and Resources (Changchun, China). The international standard zircon 91500 [46] was used as external standards to normalize isotopic fractionation and calculate the isotopic compositions. Australian Macquarie University standard zircon GJ-1 was used as a secondary standard to supervise the deviation of age measurements/calculations. The ratios of $^{206}Pb/^{238}U$, $^{207}Pb/^{235}U$, and $^{207}Pb/^{206}Pb$ were calculated with the ICPMSdatacal program (Version: 9.9) [47] and the plot of concordance and the weighted average age were made by Isoplot (Version: 3.0) [48]. The standard lead correction was based on the Andersen [49] method. For detailed experimental procedures and parameters, please see Li et al. [43,44].

3.2. Whole-Rock Major and Trace Element Analysis

Through petrographic observation, the samples were ground to 200 mesh using an agate mill, and the whole-rock major and trace geochemical analysis were completed at ALS Minerals–ALS Chemex (Guangzhou, China). The ME-XRF06 X instrument was used to determine the major elements; the trace element components were performed by ICP–AES and ICP–MS methods. During the test, we selected two international standard material samples (Canadian diorite gneiss SY-4 and kinzingite SARM-45) as calibration standards (listed in Supplementary Table S2). The analytical precision was better than 5% for the major elements and better than 10% for the trace elements [43].

3.3. Zircon Hf Isotopic Analysis

Using Neptune (MC) ICP–MS equipment equipped with a new generation up 213 laser ablation probe, the zircon in situ Hf isotopic analysis from the U-Pb dating point on the same crystal was completed in the State Key Laboratory of Isotope Geochronology and Geochemistry, Tianjin Institute of Geology and Mineral Resources (Tianjin, China). The standard zircon selected during the analysis was GJ-1, with an ablation rate of 10 Hz and a spot diameter of 45 μm. Helium was used as the carrier gas for the ablated aerosol. The $^{176}Hf/^{177}Hf$ ratio determined for the GJ-1 standard zircon was 0.282001 ± 0.000015 (n = 27). For detailed experimental operating conditions, procedures, and parameters, please refer to Geng et al. [50] and Li et al. [43].

4. Results

4.1. Zircon U-Pb Ages

We separated and analyzed 23 zircons from sample TH and 20 zircons from sample DDZ. For the representative zircons, CL images are shown in Figure 4 and the U-Pb data (Supplementary Table S1) are displayed graphically in Tera–Wasserburg diagrams (Figure 5). All of the zircon grains show obvious oscillatory growth zone and a high Th/U ratio (0.11–1.79; Supplementary Table S1), suggesting that they are of magmatic origin [51].

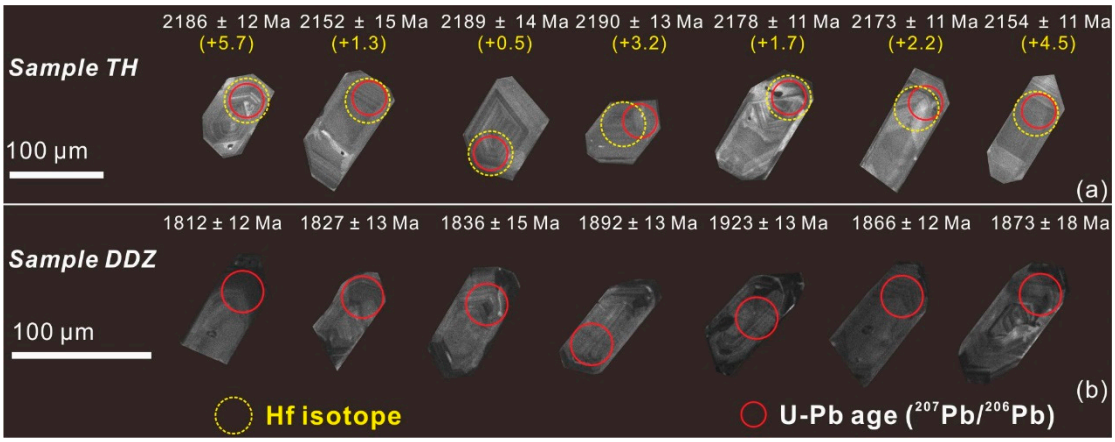

Figure 4. Cathodoluminescence images of representative zircons from magmatic rocks in the Qingchengzi district. (**a**) sample TH, (**b**) sample DDZ.

A total of 23 spots were analyzed on 23 zircon grains from sample TH (Supplementary Table S1). Seven analyses were excluded because of high discordance (>5%). The remaining 16 spots had Th/U ratios and ^{207}Pb/^{206}Pb ages varying from 1.14 to 1.71 and 2190 to 2131 Ma, respectively (Supplementary Table S1). They plot on concordia with a weighted mean ^{207}Pb/^{206}Pb age of 2163 ± 9 Ma (n = 16; MSWD = 2.0) (Figure 5a), which is interpreted as the emplacement age of the granite porphyry.

Twenty analyses were made on 20 zircon grains from sample DDZ (Supplementary Table S1). Among them, four analyses were excluded because of high discordance (>5%). The remaining 16 spots had Th/U ratios and ^{207}Pb/^{206}Pb ages varying from 0.11 to 0.46 and 1923 to 1749 Ma, respectively (Supplementary Table S1). They plot on concordia with a weighted mean ^{207}Pb/^{206}Pb age of 1854 ± 21 Ma (n = 16; MSWD = 7.7) (Figure 5b), which is interpreted as the emplacement age of the biotite granite.

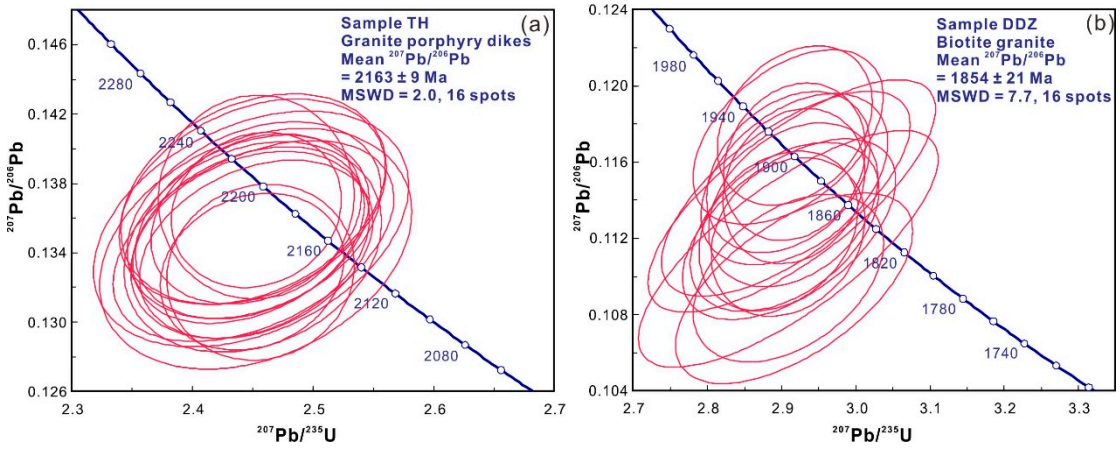

Figure 5. Concordia diagrams of LA–ICP–MS zircon U-Pb for Paleoproterozoic igneous rock in the Qingchengzi district, (**a**) sample TH, (**b**) sample DDZ.

4.2. Whole-Rock Major and Trace Element Geochemistry

The whole-rock major and trace geochemical compositions of Qingchengzi Paleoproterozoic igneous rock are listed in Supplementary Table S2. As shown in the Q–A–P (quartz–alkali feldspar–plagioclase) diagram [52], all the samples belong to the syenogranite/granite field (Figure 6a); in the SiO_2 vs. total alkali (Na_2O + K_2O; TAS) diagram [53], all fall within the granite fields (Figure 6b), which is consistent with the results of the petrographic observation.

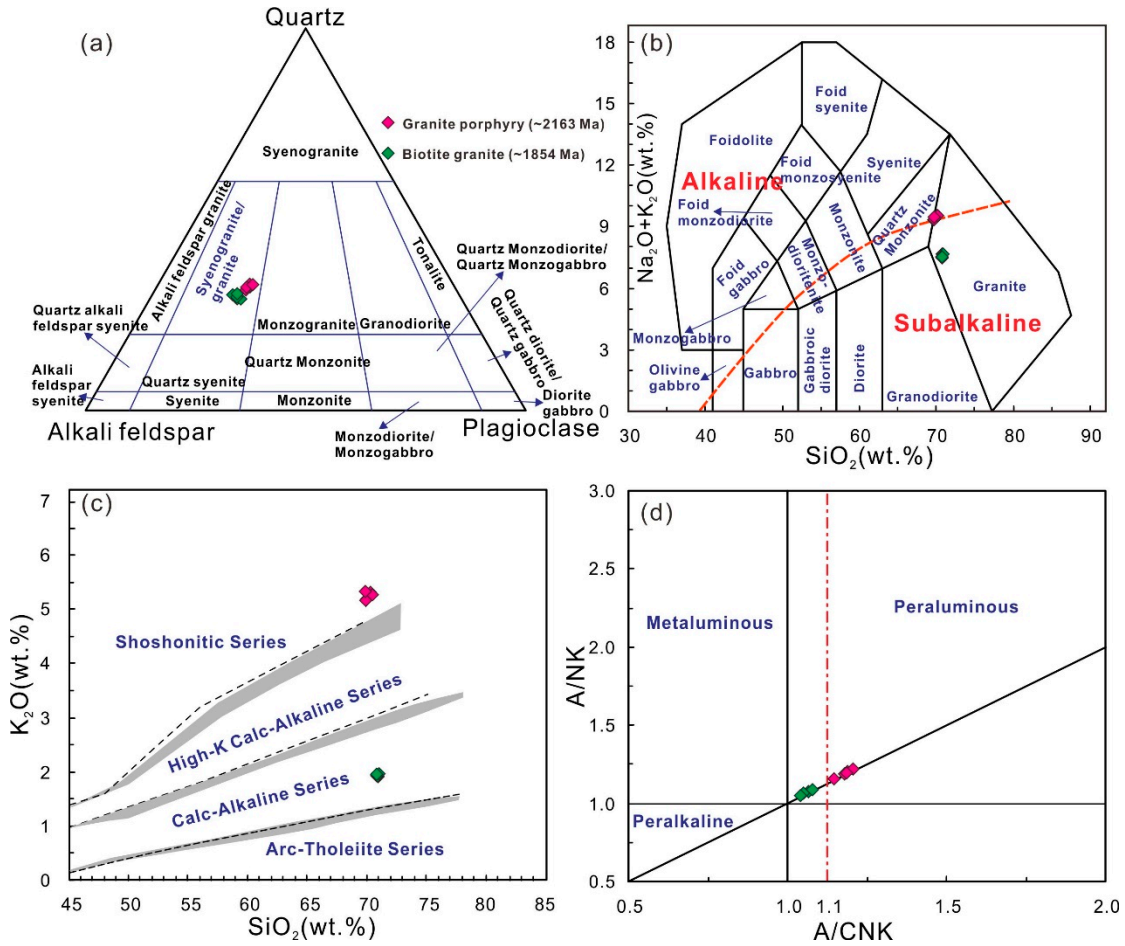

Figure 6. Major element geochemical diagram of igneous rocks in Qingchengzi district. (**a**) Modal quartz–alkali feldspar–plagioclase classification (after Le Maitre [52]); (**b**) total alkali ($Na_2O + K_2O$) vs. SiO_2 (after Irvine and Baragar [53]); (**c**) K_2O vs. SiO_2 (after Peccerillo and Taylor [54]); and (**d**) A/NK vs. A/CNK (after Maniar and Piccoli [55]).

4.2.1. Granite Porphyry (Sample TH)

Granite porphyry samples contain SiO_2 = 69.72–70.31 wt.%, total alkalis ($Na_2O + K_2O$) = 9.26–9.46 wt.%, Al_2O_3 = 15.53–15.75 wt.%, TFe_2O_3 (total) = 1.90–2.29 wt.%, CaO = 0.35–0.49 wt.%, and $Mg^{\#}$ = 48–51. These samples fall in the subalkaline series field in the SiO_2 vs. total alkali diagram (Figure 6b) and are classified as high-K calc-alkaline rocks in the K_2O vs. SiO_2 diagram (Figure 6c). Also, the A/CNK [molar $Al_2O_3/(CaO + K_2O + Na_2O)$] values of these samples are 1.15~1.21, displaying peraluminous characteristics (Figure 6d). The granite porphyry samples show the characteristics of light rare earth element (LREE) enrichment and heavy rare earth element (HREE) depletion (LREE/HREE = 31.87–33.09; La_N/Yb_N = 61.24–64.27), and negligible Eu anomalies (Eu/Eu* = 0.94–1.00) (Figure 7a). On the N-MORB (Normal-Mid Ocean Ridge Basalt) normalized trace element spider diagrams, the samples are shown to be enriched in the large-ion lithophile elements (LILEs; e.g., Rb, Cs, and K) and Ti, and depleted in the high field strength elements (HFSEs; e.g., Nb and Ta) (Figure 7b) (Supplementary Table S2).

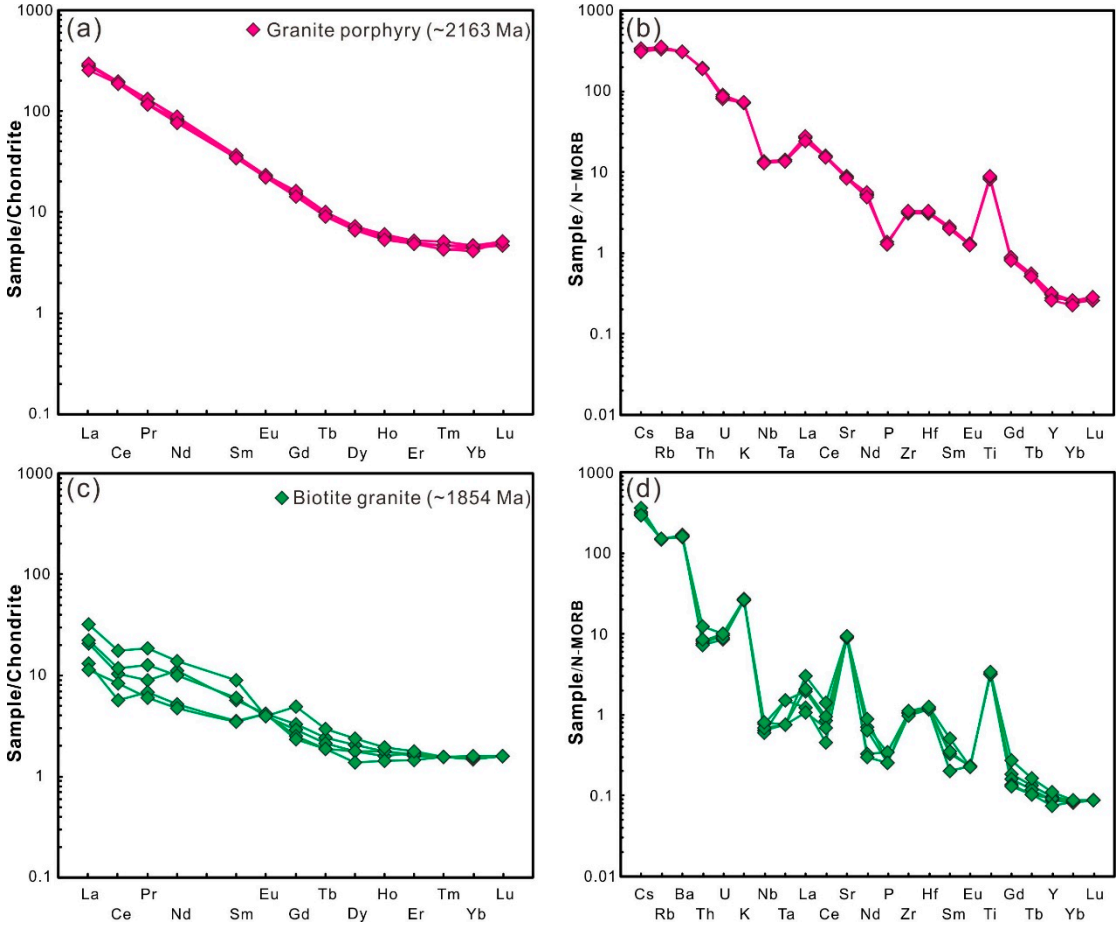

Figure 7. Trace element geochemical diagram of Paleoproterozoic igneous rocks in Qingchengzi district (Note: the normalized values of chondrite and N-MORB are from Sun and McDonough [56]). (**a**,**c**) Chondrite-normalized rare earth element patterns, (**b**,**d**) N-MORB normalized trace element patterns.

4.2.2. Biotite Granite (Sample DDZ)

The biotite granite has SiO_2 = 70.75–70.89 wt.%, total alkalis = 7.44–7.63 wt.%, Al_2O_3 = 16.51–16.78 wt.%, TFe_2O_3 (total) = 1.29–1.31 wt.%, CaO = 2.23–2.53 wt.%, and $Mg^{\#}$ = 38–40. Biotite granite belongs to the subalkaline and shoshonitic series, with A/CNK ratio between 1.04 and 1.08, showing weakly peraluminous characteristics (Figure 6b–d). Biotite granite samples are enriched in LREEs, depleted in HREEs (LREE/HREE = 6.01–11.44; La_N/Yb_N = 7.45–20.19), and exhibit varied Eu anomalies (Eu/Eu* = 0.60–1.45) (Figure 7c). In the N-MORB normalized trace element spider diagram, the biotite granite samples are shown to be enriched in LILEs (e.g., Cs, Rb, Th, and K) and Ti, and depleted in HFSEs (e.g., Nb and Ta) (Figure 7d) (Supplementary Table S2).

4.3. Zircon Hf Isotopic Compositions

In situ Hf isotopic analysis was carried out on samples that were zircon U-Pb dated, and the corresponding results are shown in Supplementary Table S3. The calculation of the two-stage model age (T_{DM2}) assumes that the average value of the continental crust $^{176}Lu/^{177}Hf$ is 0.015, and back to the depleted mantle model growth curve by calculating the initial $^{176}Hf/^{177}Hf$ [57].

The granite porphyry has an initial $^{176}Hf/^{177}Hf$ ratio of 0.281403–0.281678, T_{DM2} varying from 3109 to 2560 Ma, and an εHf(t) value that has a small variation range (−1.5 to +4.8) (Figure 8). Song et al. [58] conducted Hf isotope analysis of the biotite granite. The results showed that the initial

$^{176}Hf/^{177}Hf$ ratios are 0.281486–0.281691, the εHf(t) values range from −14.1 to +4.1, and the T_{DM2} model ages range from 3105 to 2453 Ma.

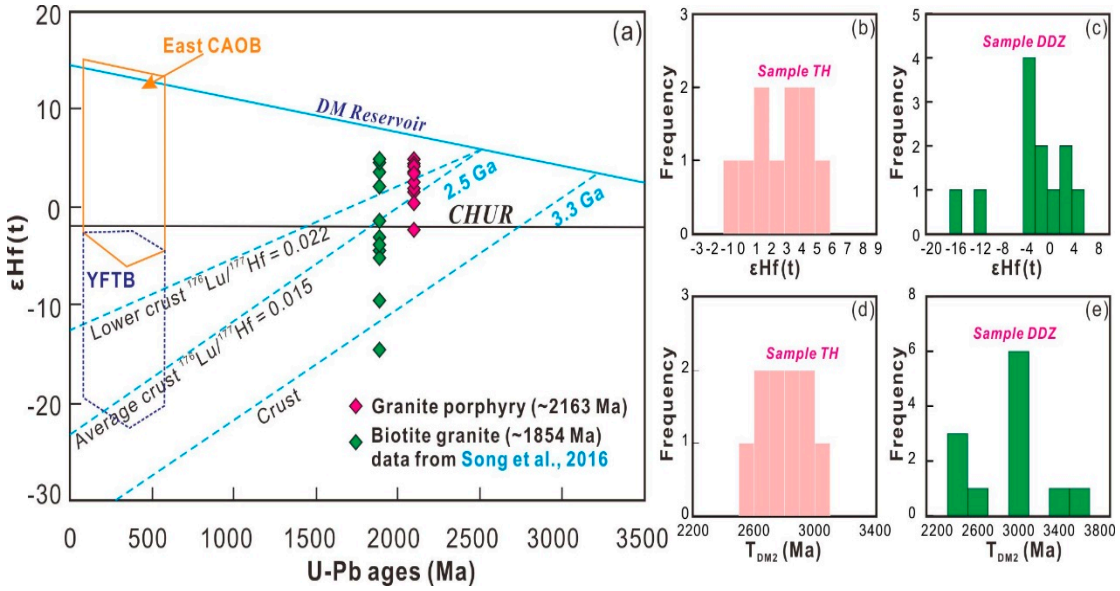

Figure 8. The εHf(t) vs. U-Pb ages (Ma) diagram for the Paleoproterozoic igneous rocks from the Qingchengzi district. Abbreviations: YFTB = Yanshan fold and thrust belt (Yang et al. [59]); CAOB = Central Asian Orogenic Belt; CHUR = chondritic uniform reservoir; DM = depleted mantle. (**a**) εHf(t) vs. U-Pb ages (Ma) diagram, (**b**,**c**) Histograms of εHf(t) values, (**d**,**e**) Histograms of T_{DM2} ages.

5. Discussion

5.1. Paleoproterozoic Magmatic Events of the Northeastern Jiao-Liao-Ji Belt

Paleoproterozoic magmatism is one of the more prominent events in the geological history of Earth, and the geodynamics and thermal state have changed globally [60]. The northeast part of the JLJB is one of the most intense areas of Paleoproterozoic magmatic-tectonism in eastern China. As shown in Figure 9, Paleoproterozoic granitoids are widely distributed in the northeastern JLJB. Therefore, the geochronological information and emplacement histories of these granites can constrain the evolution and nature of magmatism affecting the area.

In this study, the CL image demonstrates that the zircon crystals are euhedral–subhedral, with obvious oscillation growth zones (Figure 4). Furthermore, combined with the high Th/U ratios (0.11–1.79; Supplementary Table S1), the results indicate that these zircons have a magmatic origin [51]. The weighted average $^{207}Pb/^{206}Pb$ ages of these two granitoids are 2163 ± 9 and 1854 ± 21 Ma, respectively, suggesting that these granitoids were emplaced during the Paleoproterozoic. To better understand the spatial and temporal distribution characteristic of magmatic rocks in the Qingchengzi district (including adjacent areas), we collected geochronological data of the northeastern JLJB, which are plotted/listed in Figure 9 and Supplementary Table S4. There are mainly three major phases of magmatic events identified in the northeastern JLJB, i.e., (1) early stage of Paleoproterozoic (2213–2205 Ma), when the granitic gneiss, granite porphyry, and monzogranitic gneiss were emplaced; (2) early-middle stage of Paleoproterozoic (2189–2119 Ma), when abundant magmatic rocks (peak), including monzogranite, granitic gneiss, granodiorite, (biotite) granite, and syenogranite were emplaced; and (3) late stage of Paleoproterozoic (1995–1740 Ma), mainly including (quartz) diorite, (porphyritic) monzogranite, porphyritic granite, and syenite.

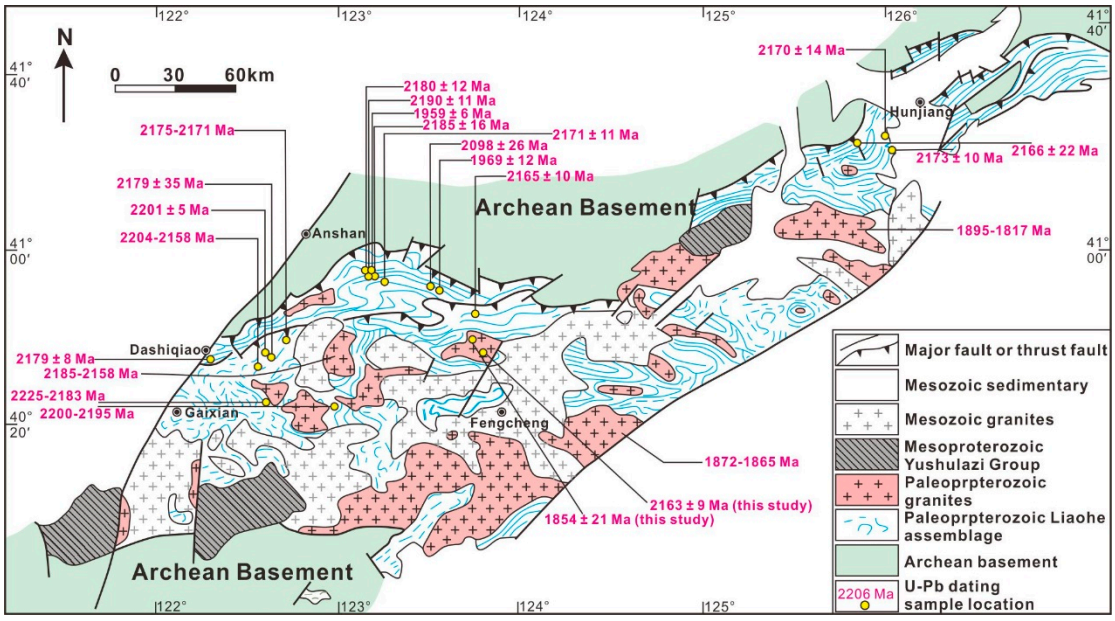

Figure 9. Geological sketch and age distribution of the northeastern Jiao-Liao-Ji Belt (modified after Bi et al. [34] and Dong et al. [35]). Note: the age data in the figure are listed in Supplementary Table S4.

5.2. Petrogenesis Models of Magmatism in the Qingchengzi District

Paleoproterozoic magmatic rocks in Qingchengzi district are similar in geochemical composition, with high Sr (760–842 ppm) and Al_2O_3 (15.53–16.78 wt.%), low Yb (0.25–0.80 ppm) and Y (2.1–9.0 ppm) contents, and show an inconspicuous Eu anomaly (Eu/Eu* = 0.60–1.45), suggesting that the Paleoproterozoic intrusions in the district have an adakite affinity (Figure 10a). Adakite can be formed in two ways: (1) partial melting of a delaminated/thickened lower crust or subducted oceanic slab [61–68] or (2) assimilation and fractional crystallization of basaltic magmas (AFC process) [69,70], or the mixing of such magmas [71].

The Paleoproterozoic intrusions in the district have low-medium $Mg^{\#}$ values and incompatible element content (e.g., Cr, Co, and Ni), among them, the $Mg^{\#}$ values (48–51) and Cr (26–27 ppm), Co (3.4–4.2 ppm), and Ni (10.8–13.2 ppm) contents in granite porphyry are slightly higher than those in biotite granite ($Mg^{\#}$ = 38–40; Cr = 11–12 ppm; Co = 1.9–2.0 ppm; Ni = 2.2–2.5 ppm), which show that the Paleoproterozoic magma may not be formed by partial melting of a delaminated lower crust or subducting oceanic slab. During these processes, mantle peridotites are inevitably entrained with magma ascending through the mantle wedge with concurrent metasomatism, and increased the magma $Mg^{\#}$ and Cr-Co-Ni contents [61,63,66]. The adakite produced by basaltic magma AFC processes usually requires a large amount of basaltic or dacitic rocks [69,70]. However, there are no mixed textures, mafic microgranular enclaves, and contemporaneous mafic rocks, which rules out the possibility of mixing from a basaltic magma or AFC process.

This indicates that the Paleoproterozoic intrusions in the district originated from the partial melting of thickened lower crust material. In the genetic discrimination diagram, these samples belong to the average crust and thickened lower crust (Figure 10b–d). According to the Hf isotope composition, the Paleoproterozoic adakitic rocks are considered to be a product of partial melting of the thickened lower crust material in the Meso-Neoarchean.

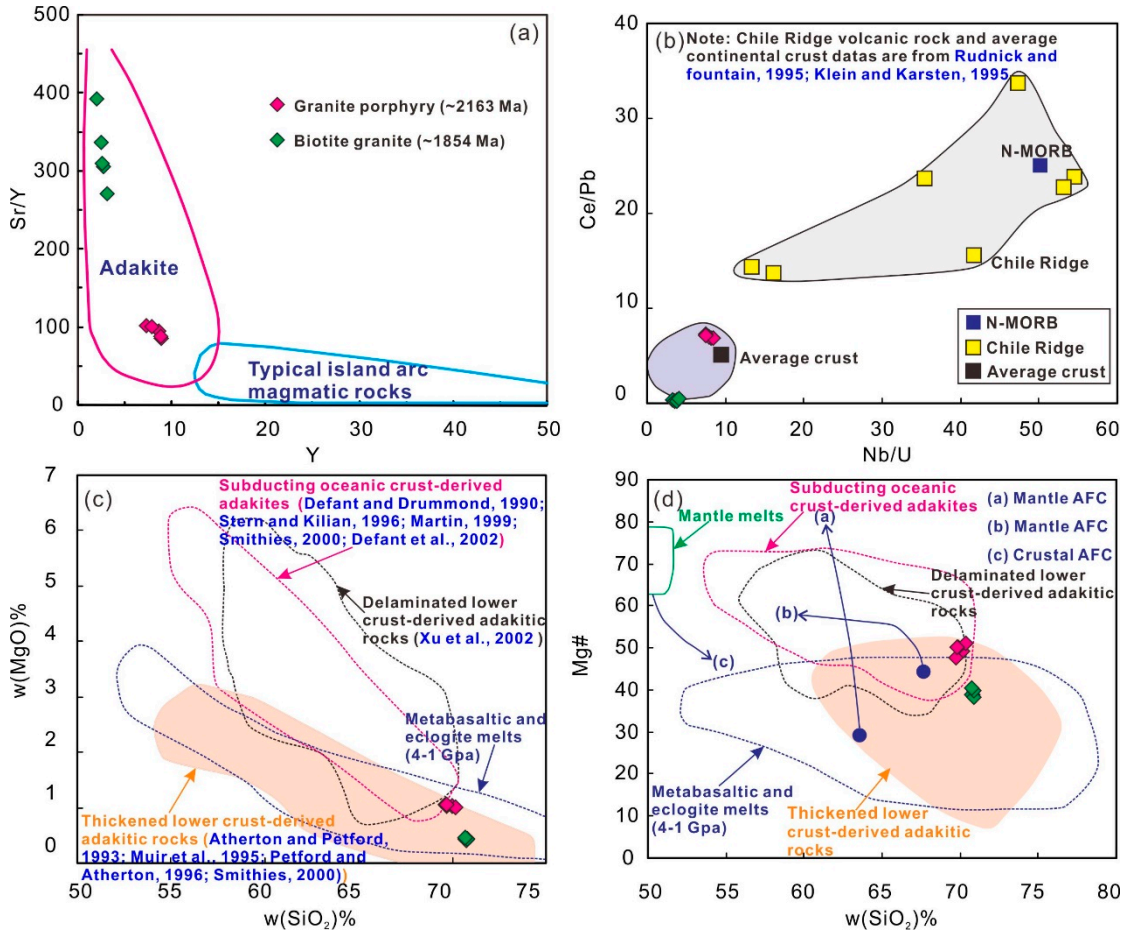

Figure 10. Discrimination diagrams of Paleoproterozoic adakitic rocks in the Qingchengzi district. (**a**) Sr/Y vs. Y (after Defant and Drummond [61]; Martin [63]); (**b**) Ce/Pb vs. Nb/U (Chile Ridge volcanic rock and average continental crust data are from Klein and Karsten [72], Rudnick and Fountain [73], Muir et al. [74]); (**c**) MgO vs. SiO_2; (**d**) $Mg^{\#}$ vs. SiO_2.

5.3. Implications for Tectonic Setting

The JLJB recorded a series of complex magma–metamorphic activities and multistage deformation events. Widely exposed Paleoproterozoic magmatic rocks (Figure 9) are the key to understanding the magmatic-tectonism of the JLJB. As summarized in Supplementary Table S4, Palaeoproterozoic granitoids have recently been reported from the JLJB. However, the evolutionary process and tectonic setting of the JLJB remain controversial, and two principal theories have been proposed, including: (1) an intracontinental rift model [7,22–27,75,76] and (2) an arc–continent collision model [28–35].

The intracontinental rift model was originally proposed by Zhang [22]. During the early stage of continental breakup, granitic magma was emplaced and formed a large number of Paleoproterozoic granites. With the increased degree of rift evolution, a large amount of mantle material upwelling formed a series of ultrabasic–basic rock bodies. This process also formed a large-scale boron-bearing rock series in the area, and the rift eventually closed between the Longgang and Namgrim blocks [22,23]. According to the systematic summary of previous studies, Li et al. [77] and Zhao et al. [3] further improved the theory of the intracontinental rift evolution based on the following pieces of evidence. (a) The Liaohe Group (e.g., the Gaixian and Li'eryu Formation) consists of a large number of greenschist to lower-amphibolite facies metamorphic basic rocks and metamorphic rhyolites, forming a bimodal volcanic assemblage [24,25,78]. In addition, A-type granites and rapakivi granites were also developed in the area [24,25,78]. (b) There are contemporaneous Tonalite-Trondhjemite-Granodiorite (TTG) gneiss basement (~2.5 Ga) and mafic rock wall (~2.46 Ga) on both sides of the JLJB [78]. (c) Li et al. [77] identified

and established deformation patterns related to extension events. (d) The geochemical characteristics of the talc deposits in the JLJB show nonmarine origin, similar to those in the Neoproterozoic Damaran Rift, South Africa [3,79,80].

Bai [28] and Faure et al. [29] suggested that the JLJB is in an active continental marginal environment, either at the northern margin of the Namgrim Block or the southern margin of the Longgang Block. In recent years, some scholars proposed that the JLJB may be a continental arc magmatic belt, based on the study of ~2.2–2.1 Ga magmatic rocks (mainly mafic and granitic intrusions), which further supports the arc–continent collision model [31,32].

The geochronological information in the two Archean–Palaeoproterozoic blocks of Longgang and Namgrim is of great importance for understanding these arguments [35]. The basement of the Longgang Block was formed at ~3.8–2.47 Ga [1,39,40,81,82], including the oldest geological unit (Anshan Group; ~3.8 Ga) [39] in China. However, no geochronological data as old as 3.8 Ga has been reported on the basement rocks of Namgrim Block [8]. Moreover, the basement rocks of the Namgrim Block show amphibolite facies metamorphism [8,41], while the Longgang Block shows amphibolite–granulite facies metamorphism [39,40]. Therefore, the geochronology and metamorphic characteristics on both sides of the JLJB are quite different, and these geological facts suggest that the intracontinental rift model is unjustified.

In summary, the whole-rock geochemical composition reported in this study shows that the Paleoproterozoic adakitic rocks in the Qingchengzi district are characterized by high Al_2O_3 and SiO_2 contents and Sr/Y ratios, LREEs and LILEs enrichment, and HREEs and HFSEs depletion (Supplementary Table S2). Combining the Hf isotopic characteristics, these granitoids are derived from the partial melting of the Meso-Neoarchean thickened lower crust material, consistent with the magmatic rocks formed in the tectonic setting of an active continental margin or island arc (e.g., [83–86]). In addition, previous studies have shown that the JLJB Paleoproterozoic volcanic rocks (e.g., Liaohe Group) are calc-alkaline series and show the characteristics of I-type granites, and they were formed in an volcanic arc environment [34]. Therefore, we suggest that the Paleoproterozoic granitoids of the JLJB were formed in an active continental margin setting, which may be related to the subduction of oceanic crust between the Namgrim and Longgang blocks.

6. Conclusions

1. Our LA–ICP–MS zircon U-Pb dating determined that the Paleoproterozoic magmatism in the Qingchengzi district occurred during two periods: ~2163 Ma (granite porphyry) and ~1854 Ma (biotite granite).
2. The Paleoproterozoic granitoids in Qingchengzi district have the affinity of adakitic rocks, which originated by partial melting of the thickened lower crust material in the Meso-Neoarchean.
3. These granitoids were formed in the tectonic setting of an active continental margin that may be related to the subduction of oceanic crust between the Namgrim and Longgang blocks.

Supplementary Materials: The following are available online at http://www.mdpi.com/2075-163X/10/8/684/s1, Table S1: LA–ICP–MS zircon U-Pb data for zircons from the Paleoproterozoic igneous rocks in Qingchengzi district, Table S2: Major (wt.%) and trace element (ppm) data for the Paleoproterozoic igneous rocks of the Qingchengzi district, Table S3: In situ zircon Hf isotopic data for the granite porphyry dike (~2163 Ma) of Qingchengzi district, Table S4: Geochronological data for the igneous rocks of the northeastern Jiao-Liao-Ji Belt.

Author Contributions: Conceptualization, J.L. and K.W.; methodology, J.L. and W.C.; validation, K.W.; formal analysis and data curation, J.L. and H.L.; project administration, K.W.; writing—original draft, J.L. All authors have read and agreed to the published version of the manuscript.

Funding: This research was funded by National Key R&D Program of China, grant number 2018YFC0603804.

Acknowledgments: We gratefully acknowledge the two anonymous reviewers for their insightful comments, which greatly improved the manuscript. We thank Francis Wu, Kimura Xia, and Jingjing Yang for their handling of the manuscript and editorial input. We would like to thank Zhigao Wang, Namhoon Kim, Gill-Jae Lee, and Bong-Chul Yoo for their assistance during fieldwork.

Conflicts of Interest: The authors declare no conflict of interest.

References

1. Wan, Y.S.; Li, R.W.; Wilde, S.A.; Liu, D.Y.; Chen, Z.Y.; Yan, L.; Song, T.R.; Yin, X.Y. UHP metamorphism and exhumation of the Dabie Orogen, China: Evidence from SHRIMP dating of zircon and monazite from a UHP granitic gneiss cobble from the Hefei Basin. *Geochim. Cosmochim. Acta* **2005**, *69*, 4333–4348. [CrossRef]
2. Wan, Y.S.; Dong, C.Y.; Jie, W.Q.; Liu, S.J.; Ma, M.Z.; Xie, S.Y.; Ren, P.; Sun, H.Y.; Liu, D.Y. Some Progress in the Study of Archean Basement of the North China Craton. *Acta. Geoscientica. Sin.* **2015**, *36*, 685–700.
3. Zhao, G.C.; Sun, M.; Wilde, S.A.; Li, S.Z. Late Archean to Paleoproterozoic evolution of the North China Craton: Key issues revisited. *Precambr. Res.* **2005**, *136*, 177–202. [CrossRef]
4. Zhao, G.C.; Li, S.Z.; Sun, M.; Wilde, S.A. Assembly, Accretion and Breakup of the Paleo-Mesoproterozoic Columbia Supercontinent: Records in the North China Craton. *Int. Geol. Rev.* **2011**, *53*, 1331–1356. [CrossRef]
5. Zhao, G.C.; Cawood, P.A.; Li, S.Z.; Wilde, S.A.; Sun, M.; Zhang, J.; He, Y.H.; Yin, C.Q. Amalgamation of the North China Craton: Key issues and discussion. *Precambr. Res.* **2012**, *222*, 55–76. [CrossRef]
6. Zhai, M.G.; Santosh, M. The early Precambrian odyssey of the North China Craton: A synoptic overview. *Gondwana Res.* **2011**, *20*, 6–25. [CrossRef]
7. Li, S.Z.; Liu, Y.J.; Yang, Z.S.; Ma, R. Continental dynamics and regional metamorphism of the Liaohe Group. *Geol. Rev.* **2001**, *47*, 9–18.
8. Lu, X.P.; Wu, F.Y.; Lin, J.Q.; Sun, D.Y.; Zhang, Y.B.; Guo, C.L. Geochronological successions of the early Precambrian granitic magmatism in southern Liaodong Peninsula and its constraints on tectonic evolution of the North China Craton. *Chin. J. Geol.* **2004**, *39*, 123–138.
9. Wan, Y.S.; Song, B.; Liu, D.Y.; Wilde, S.A.; Wu, J.S.; Yin, X.Y.; Zhou, H.Y. SHRIMP U-Pb zircon geochronology of Palaeoproterozoic metasedimentary rocks in the North China Craton: Evidence for a major Late Palaeoproterozoic tectonothermal event. *Precambr. Res.* **2006**, *149*, 249–271. [CrossRef]
10. Liu, F.L.; Liu, P.H.; Wang, F.; Liu, C.H.; Cai, J. Progresses and overviews of voluminous meta-sedimentary series within the Paleoproterozoic Jiao-Liao-Ji orogenic/mobile belt, North China Craton. *Acta Petrol. Sin.* **2015**, *31*, 2816–2846.
11. Zhao, G.C.; Wilde, S.A.; Cawood, P.A.; Lu, L.Z. Thermal evolution of the Archaean basement rocks from the eastern part of the North China Craton and its bearing on tectonic setting. *Int. Geol. Rev.* **1998**, *40*, 706–721. [CrossRef]
12. Zhao, G.C.; Wilde, S.A.; Cawood, P.A.; Sun, M. Archean blocks and their boundaries in the North China Craton: Lithological, geochemical, structural and P–T, path constraints and tectonic evolution. *Precambr. Res.* **2001**, *107*, 45–73. [CrossRef]
13. Wilde, S.A.; Zhao, G.C.; Sun, M. Development of the North China Craton during the late Archaean and its final amalgamation at 1.8 Ga: Some speculations on its position within a global Palaeoproterozoic supercontinent. *Gondwana Res.* **2002**, *5*, 85–94. [CrossRef]
14. Wilde, S.A.; Cawood, P.A.; Wang, K.; Nemchin, A.A. Granitoid evolution in the Late Archean Wutai Complex, North China Craton. *J. Asian Earth Sci.* **2005**, *24*, 597–613. [CrossRef]
15. Kröner, A.; Wilde, S.A.; Zhao, G.C.; O'Brien, P.J.; Sun, M.; Liu, D.Y.; Wan, Y.S.; Liu, S.W.; Guo, J.H. Zircon geochronology and metamorphic evolution of mafic dykes in the Hengshan Complex of northern China: Evidence for late Palaeoproterozoic extension and subsequent high-pressure metamorphism in the North China Craton. *Precambr. Res.* **2006**, *146*, 45–67. [CrossRef]
16. Yin, C.Q.; Zhao, G.C.; Sun, M.; Xia, X.P.; Wei, C.J.; Zhou, X.W.; Leung, W.H. LA-ICP-MS U-Pb zircon ages of the Qianlishan Complex: Constrains on the evolution of the Khondalite Belt in the Western Block of the North China Craton. *Precambr. Res.* **2009**, *174*, 78–94. [CrossRef]
17. Yin, C.Q.; Zhao, G.C.; Guo, J.H.; Sun, M.; Xia, X.P.; Zhou, X.W.; Liu, C.H. U-Pb and Hf isotopic study of zircons of the Helanshan Complex: Constrains on the evolution of the Khondalite Belt in the Western Block of the North China Craton. *Lithos* **2011**, *122*, 25–38. [CrossRef]
18. Santosh, M. Assembling North China Craton within the Columbia supercontinent: The role of double-sided subduction. *Precambr. Res.* **2010**, *178*, 149–167. [CrossRef]
19. Li, X.P.; Yang, Z.; Zhao, G.; Grapes, R.; Guo, J. Geochronology of khondalite-series rocks of the Jining Complex: Confirmation of depositional age and tectonometamorphic evolution of the North China craton. *Int. Geol. Rev.* **2010**, *53*, 1194–1211. [CrossRef]

20. Santosh, M.; Liu, S.J.; Tsunogae, T.; Li, J.H. Paleoproterozoic ultrahigh-temperature granulites in the North China Craton: Implications for tectonic models on extreme crustal metamorphism. *Precambr. Res.* **2012**, *222*, 77–106. [CrossRef]
21. Santosh, M.; Liu, D.Y.; Shi, Y.R.; Liu, S.J. Paleoproterozoic accretionary orogenesis in the North China Craton: A SHRIMP zircon study. *Precambr. Res.* **2013**, *227*, 29–54. [CrossRef]
22. Zhang, Q.S. *Geology and Metallogeny at Early Proterozoic in China*; Jilin People's Press: Changchun, China, 1984; pp. 1–536.
23. Zhang, Q.S. *Early Crust and Deposit of Eastern Liaoning Peninsula*; Geological Publishing House: Beijing, China, 1988; pp. 1–574.
24. Sun, M.; Armstrong, R.L.; Lambert, R.S.J.; Jiang, C.B.; Wu, J.H. Petrochemistry and Sr, Pb and Nd isotopic geochemistry of the paleoproterozoic kuandian complex, the eastern Liaoning province, China. *Precambr. Res.* **1993**, *62*, 171–190.
25. Peng, Q.M.; Palmer, M.R. The Palaeoproterozoic boron deposits in eastern Liaoning, China: A metamorphosed evaporite. *Precambr. Res.* **1995**, *72*, 185–197. [CrossRef]
26. Liu, J.L.; Liu, Y.J.; Chen, H.; Sha, D.M.; Wang, H.C. The inner zone of the Liaoji paleorift: Its early structural styles and structural evolution. *J. Asian Earth Sci.* **1997**, *15*, 19–31. [CrossRef]
27. Li, S.Z.; Liu, Y.J. Palaeoproterozoic sedimentary assemblages in the Jiao-Liao Massif: Ages and stratigraphic sequence. *Northwestern Geol.* **1997**, *18*, 13–20.
28. Bai, J.; Huang, X.G.; Dai, F.Y.; Wu, C.H. *The Precambrian Evolution of China*; Geological Publishing House: Beijing, China, 1993; pp. 199–203.
29. Faure, M.; Lin, W.; Monie, P.; Bruguier, O. Paleoproterozoic arc magmatism and collision in Liaodong Peninsula (north-east China). *Terra Nova* **2004**, *16*, 75–80. [CrossRef]
30. Ma, L.J.; Cui, Y.C.; Liu, J.L.; Zhang, J.B. Geochemical Characteristics and the Tectonic Setting of Amphibolites of the North Liaohe Group in Liaodong Area. *J. Shanxi Univ. (Nat. Sci. Ed.)* **2007**, *30*, 515–523.
31. Li, Z.; Chen, B. Geochronology and geochemistry of the Paleoproterozoic meta-basalts from the Jiao-Liao-Ji Belt, North China Craton: Implications for petrogenesis and tectonic setting. *Precambr. Res.* **2014**, *255*, 653–667. [CrossRef]
32. Yuan, L.L.; Zhang, X.H.; Xue, F.H.; Han, C.M.; Chen, H.L.; Zhai, M.G. Two episodes of Paleoproterozoic mafic intrusions from Liaoning province, North China Craton: Petrogenesis and tectonic implications. *Precambr. Res.* **2015**, *264*, 119–139. [CrossRef]
33. Yang, M.C.; Chen, B.; Yan, C. Petrogenesis of Paleoproterozoic gneissic granites from Jiao-Liao-Ji Belt of North China Craton and their tectonic implications. *J. Earth Sci. Environ.* **2015**, *37*, 31–51.
34. Bi, J.H.; Ge, W.C.; Xing, D.H.; Yang, H.; Dong, Y.; Tian, D.X.; Chen, H.J. Palaeoproterozoic meta-rhyolite and meta-dacite of the Liaohe Group, JiaoLiao-Ji Belt, North China Craton: Petrogenesis and implications for tectonic setting. *Precambr. Res.* **2018**, *314*, 306–324. [CrossRef]
35. Dong, Y.; Bi, J.H.; Xing, D.H.; Ge, W.C.; Yang, H.; Hao, Y.J.; Ji, Z.; Jing, Y. Geochronology and geochemistry of Liaohe Group and Liaoji granitoid in the Jiao-Liao-Ji Belt, North China Craton: Implications for petrogenesis and tectonic evolution. *Precambr. Res.* **2019**, *332*, 105399. [CrossRef]
36. Whalen, J.B.; Currie, K.L.; Chappell, B.W. A-type granites: Geochemical characteristics, discrimination and petrogenesis. *Contrib. Miner. Petrol.* **1987**, *95*, 407–419. [CrossRef]
37. Eby, G.N. Chemical subdivision of the A-type granitoids: Petrogenetic and tectonic implications. *Geology* **1992**, *20*, 641–644. [CrossRef]
38. Pearce, J.A. Sources and settings of granitic rocks. *Episodes* **1996**, *4*, 120–125. [CrossRef]
39. Liu, D.Y.; Nutman, A.P.; Compston, W.; Wu, J.S.; Shen, Q.H. Remnants of ≥3800 Ma crust in the Chinese part of the SinoKorean Craton. *Geology* **1992**, *20*, 339–342. [CrossRef]
40. Song, B.; Nutman, A.P.; Liu, D.Y.; Wu, J.S. 3800–2500 Ma crustal evolution in the Anshan area of Liaoning Province, northeastern China. *Precambr. Res.* **1996**, *78*, 79–94. [CrossRef]
41. Lu, X.P.; Wu, F.Y.; Guo, J.H.; Wilde, S.A.; Yang, J.H.; Liu, X.M.; Zhang, X.O. Zircon U-Pb geochronological constraints on the Paleoproterozoic crustal evolution of the Eastern block in the North China Craton. *Precambr. Res.* **2006**, *146*, 138–164. [CrossRef]
42. Zhao, G.C.; Cawood, P.A. Precambrian geology of China. *Precambr. Res.* **2012**, *222*, 13–54. [CrossRef]

43. Li, J.; Cai, W.Y.; Wang, K.Y.; Kim, N.H.; Liu, H.L.; Lee, J.G.; Yoo, B.C. Initial decratonization of the eastern North China Craton: New constraints from geochronology, geochemistry, and Hf isotopic compositions of Mesozoic igneous rocks in the Qingchengzi district. *Geol. J.* **2020**, *55*, 3796–3820. [CrossRef]
44. Li, J.; Cai, W.Y.; Li, B.; Wang, K.Y.; Liu, H.L.; Yassa, K.; Qian, Y.; Lee, J.G.; Yoo, B.C. Paleoproterozoic SEDEX-type stratiform mineralization overprinted by Mesozoic vein-type mineralization in the Qingchengzi Pb-Zn deposit, Northeastern China. *J. Asian Earth Sci.* **2019**, *184*, 104009. [CrossRef]
45. Li, J.; Wang, K.Y.; Cai, W.Y.; Sun, F.Y.; Liu, H.L.; Fu, L.J.; Qian, Y.; Lai, C.K. Triassic gold-silver metallogenesis in Qingchengzi orefield, North China Craton: Perspective from fluid inclusions, REE and H-O-S-Pb isotope systematics. *Ore Geol. Rev.* **2020**, *121*, 103567. [CrossRef]
46. Wiedenbeck, M.; Allé, P.; Corfu, F.; Griffin, W.L.; Meier, M.; Oberli, F.; Quadt, V.A.; Roddick, J.C.; Spiegel, W. Three natural zircon standards for U-Th-Pb, Lu-Hf, trace element and REE analyses. *Geostand. Newsl.* **1995**, *19*, 1–23. [CrossRef]
47. Liu, Y.S.; Gao, S.; Hu, Z.C.; Gao, C.G.; Zong, K.Q.; Wang, D.B. Continental and oceanic crust recycling-induced melt-peridotite interactions in the Trans-North China Orogen: U-Pb dating, Hf isotopes and trace elements in zircons of mantle xenoliths. *J. Petrol.* **2010**, *51*, 537–571. [CrossRef]
48. Ludwig, K.R. User's manual for isoplot 3.0: A geochronological toolkit for Microsoft Excel. *Berkeley Geochronol. Center Spec. Publ.* **2003**, *4*, 1–70.
49. Andersen, T. Correction of common lead in U-Pb analyses that do not report ^{204}Pb. *Chem. Geol.* **2002**, *192*, 59–79. [CrossRef]
50. Geng, J.Z.; Qiu, K.F.; Gou, Z.Y.; Yu, H.C. Tectonic regime switchover of Triassic Western Qinling Orogen: Constraints from LA-ICP-MS zircon U-Pb geochronology and Lu–Hf isotope of Dangchuan intrusive complex in Gansu, China. *Chem. Erde.* **2017**, *77*, 637–651. [CrossRef]
51. Hoskin, P.W.O.; Black, L.P. Metamorphic zircon formation by solid-state recrystallization of protolith igneous zircon. *J. Metamorphic Geol.* **2000**, *18*, 423–439. [CrossRef]
52. Le Maitre, R.W. *Igneous Rocks. A Classification and Glossary of Terms*; Cambridge University Press: Cambridge, UK, 2002; pp. 1–236.
53. Irvine, T.H.; Baragar, W.R.A. A guide to the chemical classification of the common volcanic rocks. *Can. J. Earth. Sci.* **1971**, *8*, 523–548. [CrossRef]
54. Peccerillo, A.; Taylor, D.R. Geochemistry of Eocene calc-alkaline volcanic rocks from the Kastamonu Area, Northern Turkey. *Contrib. Miner. Petrol.* **1976**, *58*, 63–81. [CrossRef]
55. Maniar, P.D.; Piccoli, P.M. Tectonic discrimination of granitoids. *Geol. Soc. Am. Bull.* **1989**, *101*, 635–643. [CrossRef]
56. Sun, S.S.; McDonough, W.F. Chemical and isotopic systematics of oceanic basalts: Implications for mantle composition and processes. In *Magmatism in Ocean Basins*; Saunders, A.D., Norry, M.J., Eds.; Geological Society Special Publications: London, UK, 1989; Volume 42, pp. 313–345.
57. Griffin, W.L.; Wang, X.; Jackson, S.E.; Pearson, N.J.; O'Reilly, S.Y.; Xu, X.S.; Zhou, X.M. Zircon chemistry and magma mixing, SE China: In-situ analysis of Hf isotopes, Tonglu and Pingtan igneous complexes. *Lithos* **2002**, *61*, 237–269. [CrossRef]
58. Song, Y.H.; Yang, F.C.; Yan, C.L.; Wei, M.H.; Shi, S.S. SHRIMP U-Pb ages and Hf isotopic compositions of Paleoproterozoic granites from eastern part of Liaoning Province and their tectonic significance. *Acta Geol. Sin.* **2016**, *90*, 2620–2636.
59. Yang, J.H.; Wu, F.Y.; Shao, J.A.; Wilde, S.A.; Xie, L.W.; Liu, X.M. Constraints on the timing of uplift of the Yanshan Fold and Thrust Belt, North China. *Earth Planet. Sci. Lett.* **2006**, *246*, 336–352. [CrossRef]
60. Li, S.Z.; Zhao, G.C.; Santosh, M.; Liu, X.; Dai, L.M. Palaeoproterozoic tectonothermal evolution and deep crustal processes in the Jiao–Liao–Ji Belt, North China Craton: A review. *Geol. J.* **2011**, *46*, 525–543. [CrossRef]
61. Defant, M.J.; Drummond, M.S. Derivation of some modern arc magmas by melting of young subducted lithosphere. *Nature* **1990**, *347*, 662–665. [CrossRef]
62. Stern, C.R.; Kilian, R. Role of the subducted slab, mantle wedge and continental crust in the generation of adakites from the Austral Volcanic Zone. *Contrib. Miner. Petrol.* **1996**, *123*, 263–281. [CrossRef]
63. Martin, H. Adakitic magmas: Modern analogues of Archean granitoids. *Lithos* **1999**, *46*, 411–429. [CrossRef]
64. Smithies, R.H. The Archean tonalite–trondhjemite–granodiorite (TTG) series is not an analogue of Cenozoic adakite. *Earth Planet. Sci. Lett.* **2000**, *182*, 115–125. [CrossRef]

65. Defant, M.J.; Xu, J.F.; Kepezhinskas, P.; Wang, Q.; Zhang, Q.; Xiao, L. Adakites: Some variations on a theme. *Acta Petrol. Sin.* **2002**, *18*, 129–142.
66. Xu, J.F.; Shinjo, R.; Defant, M.J.; Wang, Q.; Papp, R.P. Origin of Mesozoic adakitic intrusive rock in the Ningzhen area of east China: Partial melting of delaminated lower continental crust? *Geology* **2002**, *30*, 1111–1114. [CrossRef]
67. Atherton, M.P.; Petford, N. Generation of sodium-rich magmas from newly underplated basaltic crust. *Nature* **1993**, *362*, 144–146. [CrossRef]
68. Stevenson, R.K.; David, J.; Parent, M. Crust evolution of the western Minto Block, northern Superior Province, Canada. *Precambr. Res.* **2006**, *145*, 229–242. [CrossRef]
69. Castillo, P.R.; Janney, P.E.; Solidum, R.U. Petrology and geochemistry of Camiguin Island, southern Philippines: Insights to the source of adakites and other lavas in a complex arc setting. *Contrib. Miner. Petrol.* **1999**, *134*, 33–51. [CrossRef]
70. Macpherson, C.G.; Dreher, S.T.; Thirlwall, M.F. Adakites without slab melting: High pressure differentiation of island arc magma, Mindanao, the Philippines. *Earth Planet. Sci. Lett.* **2006**, *243*, 581–593. [CrossRef]
71. Streck, M.J.; Leeman, W.P.; Chesley, J. High-magnesian andesite from Mount Shasta: A product of magma mixing and contamination, not a primitive mantle melt. *Geology* **2007**, *35*, 351–354. [CrossRef]
72. Klein, E.M.; Karsten, J.L. Ocean–ridge basalts with convergent-margin geochemical affinities from the Chile ridge. *Nature* **1995**, *374*, 52–57. [CrossRef]
73. Rudnick, R.L.; Fountain, D.M. Nature and compositions of the continental crust: A lower crustal perspective. *Rev. Geophys.* **1995**, *33*, 267–309. [CrossRef]
74. Muir, R.J.; Weaver, S.D.; Bradshaw, J.D.; Eby, G.N.; Evans, J.A. Geochemistry of the Cretaceous Separation Point Batholith, New Zealand: Granitoid magmas formed by melting of mafic lithosphere. *J. Geol. Soc.* **1995**, *152*, 689–701. [CrossRef]
75. Li, S.Z.; Hao, D.F.; Han, Z.Z.; Zhao, G.C.; Sun, M. Paleoproterozoic deep processes and tectono-thermal evolution in Jiao-Liao Massif. *Acta Geol. Sin.* **2003**, *77*, 328–340.
76. Luo, Y.; Sun, M.; Zhao, G.C.; Li, S.Z.; Xu, P.; Ye, K.; Xia, X.P. LA-ICP-MS U-Pb zircon ages of the Liaohe Group in the Eastern Block of the North China Craton: Constraints on the evolution of the Jiao-Liao-Ji Belt. *Precambr. Res.* **2004**, *134*, 349–371. [CrossRef]
77. Li, S.Z.; Zhao, G.C.; Sun, M.; Han, Z.H.; Luo, Y.; Hao, D.F.; Xia, X.P. Deformation history of the Paleoproterozoic Liaohe assemblage in the eastern block of the North China Craton. *J. Asian Earth Sci.* **2005**, *24*, 659–674. [CrossRef]
78. Zhang, Q.S.; Yang, Z.S. *Early Crust and Mineral. Deposits of Liaodong Peninsula*; Geological Publishing House: Beijing, China, 1988; pp. 218–450.
79. Jiang, S.Y.; Palmer, M.R.; Peng, Q.M.; Yang, J.H. Chemical and stable isotopic compositions of Proterozoic metamorphosed evaporites and associated tourmalines from the Houxianyu borate deposit, eastern Liaoning, China. *Chem. Geol.* **1997**, *135*, 189–211. [CrossRef]
80. Peng, Q.M.; Palmer, M.R.; Lu, J.W. Geology and geochemistry of the Paleoproterozoic borate deposits in Liaoning-Jilin, northeastern China: Evidence of meta-evaporites. *Hydrobiologia* **1998**, *381*, 51–57. [CrossRef]
81. Grant, M.L.; Wilde, S.A.; Wu, F.Y.; Yang, J.H. The application of zircon cathodoluminescence imaging, Th-U-Pb chemistry and U-Pb ages in interpreting discrete magmatic and high-grade metamorphic events in the North China Craton at the Archean/Proterozoic boundary. *Chem. Geol.* **2009**, *261*, 155–171. [CrossRef]
82. Wang, W.; Liu, S.W.; Cawood, P.A.; Bai, X.; Guo, R.R.; Guo, B.R.; Wang, K. Late Neoarchean subduction-related crustal growth in the Northern Liaoning region of the North China Craton: Evidence from ~2.55 to 2.50 Ga granitoid gneisses. *Precambr. Res.* **2016**, *281*, 200–223. [CrossRef]
83. Li, J.; Cai, W.Y.; Fu, L.J.; Zhang, X.B.; Wang, K.Y.; Ma, X.L.; Sun, Y.C. Genesis and tectonic setting of the Bulage Pb–Zn deposit, Inner Mongolia, China: Evidence from geology, fluid inclusions, EMPA, H-O isotope systematics, zircon U-Pb geochronology, and geochemistry. *Geol. J.* **2020**, *55*, 344–371. [CrossRef]
84. Li, J.; Wang, K.Y.; Fu, L.J.; Zhang, M.; Liu, H.L.; Liu, Q.Z.; Tang, W.H.; Wang, C.H. Adakitic rocks and A-type felsic dykes in the Changlingzi area. NE China: Constraints on multistage tectonism in the southern Great Xing'an Range. *Geol. J.* **2020**. [CrossRef]

85. Cai, W.Y.; Wang, Z.G.; Li, J.; Fu, L.J.; Wang, K.Y.; Yassa, K.; Li, S.D. Zircon U-Pb and molybdenite Re-Os geochronology and geochemistry of Jinchang porphyry gold-copper deposit, NE China: Two-phase mineralization and the tectonic setting. *Ore Geol. Rev.* **2019**, *107*, 735–753. [CrossRef]
86. Cai, W.Y.; Wang, K.Y.; Li, J.; Fu, L.J.; Lai, C.K.; Liu, H.L. Geology, geochronology and geochemistry of large Duobaoshan Cu-Mo-Au orefield in NE China: Magma genesis and regional tectonic implications. *Geosci. Front.* **2020**. [CrossRef]